Mathematical Biosciences and Engineering

http://www.aimspress.com/journal/mbe

MBE, 21(4): 5536–5555.
DOI: 10.3934/mbe.2024244
Received: 05 January 2024
Revised: 28 February 2024
Accepted: 05 March 2024
Published: 27 March 2024

Research article

Mechanistic modeling of alarm signaling in seed-harvester ants

Michael R. Lin[1], Xiaohui Guo[2,*], Asma Azizi[3], Jennifer H. Fewell[4] and Fabio Milner[1,5]

[1] Simon A. Levin Mathematical, Computational and Modeling Sciences Center, Arizona State University, Tempe 85281, USA
[2] Department of Physics of Complex Systems, Weizmann Institute of Science, Rehovot 7632706, Israel
[3] Department of Mathematics, Kennesaw State University, Marietta 30062, USA
[4] School of Life Sciences, Arizona State University, Tempe 85287, USA
[5] School of Mathematical and Statistical Sciences, Arizona State University, Tempe 85287, USA

* **Correspondence:** Email: xiaohui.guo@weizmann.ac.il.

Abstract: Ant colonies demonstrate a finely tuned alarm response to potential threats, offering a uniquely manageable empirical setting for exploring adaptive information diffusion within groups. To effectively address potential dangers, a social group must swiftly communicate the threat throughout the collective while conserving energy in the event that the threat is unfounded. Through a combination of modeling, simulation, and empirical observations of alarm spread and damping patterns, we identified the behavioral rules governing this adaptive response. Experimental trials involving alarmed ant workers (*Pogonomyrmex californicus*) released into a tranquil group of nestmates revealed a consistent pattern of rapid alarm propagation followed by a comparatively extended decay period [1]. The experiments in [1] showed that individual ants exhibiting alarm behavior increased their movement speed, with variations in response to alarm stimuli, particularly during the peak of the reaction. We used the data in [1] to investigate whether these observed characteristics alone could account for the swift mobility increase and gradual decay of alarm excitement. Our self-propelled particle model incorporated a switch-like mechanism for ants' response to alarm signals and individual variations in the intensity of speed increased after encountering these signals. This study aligned with the established hypothesis that individual ants possess cognitive abilities to process and disseminate information, contributing to collective cognition within the colony (see [2] and the references therein). The elements examined in this research support this hypothesis by reproducing statistical features of the empirical speed distribution across various parameter values.

Keywords: alarm response; collective behavior; ant colony; agent-based model; information dissemination

1. Introduction

The "alarm response" commonly employed by social insect colonies, serves as a vivid metaphor for a diverse range of prototypical infection processes, including rumor spread [3], social contagion [4, 5], and disease outbreaks [6]. In the case of harvester ants, for instance, a localized disturbance, such as a single intruder entering the nest, can prompt workers to adopt a distinct behavioral alarm state. In this state, they exhibit more animated movement patterns and increased contact rates with nestmates [7]. Workers often transmit this heightened state to nearby peers through direct contact and associated alarm pheromones (Ketone 4-Methyl-3-heptanone) [8–11]. Under certain conditions, this process initiates an alarm signaling cascade, resulting in a collective behavioral shift toward more turbulent motion—the colony alarm response. At its peak, the alarm response can trigger a qualitative shift in colony behavior, leading to attacks on invaders or the abandonment of the nest space. However, when the threat is unfounded, the alarm response quickly subsides to pre-alarm activity levels [1]. The physical contacts associated with the diffusion-modulated pattern of alarm information contribute to the amplification, flow, and dampening of the alarm response, making it a valuable model for understanding transmission and infection processes at various scales. Examples include infectious disease epidemics (see [12] and the references therein), the spread of viral content in online networks [13], immune responses to targets such as viruses or tumor cells [14–18], and biochemical cascades such as apoptosis [19], where local interactions magnify a small stimulus until systemic changes occur.

In contrast to numerous similar cases, the response to colony alarms is highly manageable from an empirical perspective, despite receiving limited attention regarding its practicality as a real-world experimental context for investigating information cascades. In a laboratory setting, alarm behavior can be consistently induced by introducing pre-alarmed ants to a tranquil colony, as documented by Guo et al. [1]. This can be achieved by confining ants to a two-dimensional surface, allowing for individual tracking through multi-object tracking software, such as ABCtracker [20]. The primary behavioral change observed in individual ants during an alarm event is a rapid increase in speed, coupled with heightened interactions with colony mates. By interpreting high speed as a proxy for alarm excitement, we can analyze the propagation of an alarm stimulus through the group by studying its impact on speed distribution.

Using the object tracking apparatus, spatially explicit agent-based models, such as self-propelled particles, are highly effective for investigating group-level alarm responses. In self-propelled particle models, collective motion is emulated by representing individuals as particles navigating through space and engaging in interactions [21–25]. Each entity adjusts its speed and heading direction based on local interactions with others [26]. These models offer utility by enabling the specification and assessment of motion rules at the individual level, with subsequent comparisons between simulated group-level outcomes and empirical observations.

In this study, we introduced artificially alarmed worker ants of the species *P. californicus* to inactive colonies and monitored the response of each colony by analyzing its speed distribution. Upon encountering an alarm signal, individual ants exhibited varying responses; some displayed subtle changes in behavior, while others transitioned into an alarmed state characterized by increased contact with nestmates and the transmission of alarm signals. This diversity in individual responses likely plays a crucial role in shaping the colony's ability to amplify or mitigate its overall response to alarms. Colonies responding to alarm events exhibited distinctive increases in speed and associated

speed variance, followed by a gradual decline in speeds, as outlined in previous research [1]. The modulation of collective alarm responses by physical contact between alarmed and unalarmed individuals contributes to the differentiation of genuine alarm events from false alarms. Consequently, we inquired whether these specific characteristics of group dynamics can be explained by a simple set of rules governing how individuals adjust their speeds.

Drawing on empirical observations, we developed a self-propelled particle model that incorporates contact-based mechanisms for alarm signal transmission and speed modification at the individual level. The model enables virtual ants to move at various speeds within a circular region. When an alarmed ant encounters an unalarmed ant, the latter responds by 1) increasing its walking speed and direction by explicitly defined amounts and 2) gaining the ability to transmit the alarmed state to others. Our findings indicate that this minimal model effectively replicates the observed empirical speed dynamics across a broad range of parameters. The strong alignment between our empirical and modeling approaches can also contribute to a more comprehensive understanding, such as in the context of infection and signal transduction within groups.

In the subsequent sections, we elucidate the self-propelled particle model, employing empirical distributions derived from our alarm inducement experiments. Following that, we elaborate on the materials and methods used in these experiments. Lastly, we substantiate the validity of our model by comparing its outputs to the corresponding quantities observed in the experimental results.

2. Mathematical model

We employed the self-propelled particle modeling framework to elucidate how ants react to alarm signals in relation to changes in velocity. Additionally, we investigated whether these individual responses can collectively represent an alarm response at the colony level. The model's underlying assumptions focused on three key aspects of the alarm transmission mechanism: 1) the influence of receiving alarm information on movement, 2) variations in acceleration response among ants, and 3) the process by which alarmed ants reduce their speed back to normal levels.

To address the initial inquiry, we categorized ants into a binary state: either "alarmed" or 1 "unalarmed." When unalarmed ants come into close contact with alarmed nestmates, more than 80% of them transition to an alarmed state and simultaneously increase their speed within 1.51 seconds, as noted by Guo et al. [1]. This finding implies that an immediate speed surge yields more realistic outcomes than allowing ants to accumulate speed gradually over multiple contacts and signals. Regarding the second query, we posited that each ant can enhance its speed by an individual-specific amount upon receiving an alarm signal. Our empirical findings suggested that while the transmission of alarm information generally boosts speed, it does not uniformly result in a complete transition to a qualitatively "alarmed" behavioral state for all individuals receiving the signal [1]. Thus, despite the binary nature of the state change, the degree of response in speed should exhibit variability. Finally, we assumed that ants decrease their speed at a rate directly proportional to their current speed, ensuring a prioritization of energy conservation in the absence of alarm stimuli.

2.1. Model description

We simulated a group of N ant workers navigating a two-dimensional circular arena with a radius of $M = 520$ pixels in continuous space (see Figure S1 in the Supplementary file). Our time scale was limited to just a few minutes, negating the need to account for birth or death processes.

Let λ^* represent the colony's baseline speed in the unalarmed state. Ants were consecutively numbered from 1 to N for unique identification. For each ant indexed by p ($1 \leq p \leq N$), its complete set of attributes at time-step t is denoted by

$$\phi_t^p = (x_t^p, y_t^p, \theta_t^p, A_t^p, s_t^p, \Lambda^p, \lambda_t^p),$$

where

- x_t^p and y_t^p represent the ant's spatial location in the arena at the end of time-step t, with Cartesian coordinates based on the origin at the center of the arena;
- θ_t^p denotes the angle of the ant's heading during time-step t, defined as the counterclockwise angle from the x-axis of the vector connecting two consecutive positions (see Figure S2 in the Supplementary file);
- $A_t^p \in [0, 1]$ indicates the alarm state during time-step t;
- s_t^p represents the length of the step that ant-p takes at time-step t divided by the length of the time-step (see Figure S2 in the Supplementary file). Henceforth, any s-value will be simply referred to as "speed".
- λ_t^p represents the expected value of ant-p's speed during time-step t;
- $\Lambda^p \in [0, \Lambda_{max}]$ is ant-p's *speed jump* parameter, indicating the amount by which λ_t^p increases when an ant becomes alarmed.

Some of an ant's characteristic parameters exhibited values distributed as follows:

1) **Change in Heading ($\Delta\theta_t^p$):** The alteration in heading, $\Delta\theta_t^p = \theta_t^p - \theta_{t-1}^p$, is randomly sampled at each time-step t for each ant p. Based on the empirical distribution of turning angles $\Delta\theta_t^p$ (visualized in Figure S3), our model assumes that the values of $\Delta\theta_t^p$ are sampled from a Laplace distribution (probability density function),

$$P(\Delta\theta_t^p) = \frac{\omega \exp(-\omega|\Delta\theta_t^p|)}{2}, \qquad \Delta\theta_t^p \in (-\pi, \pi), \tag{2.1}$$

where ω^{-1} signifies the mean magnitude of the turning angle, consistent for all ants across all time-steps. The adjustment of heading influences correlated random walks in ants, as observed in individual ant movement data collected from empirical videos (refer to Figure S3 in the Supplementary file and experiments in [1]).

2) **Alarm State:** In our model, "alarm" denotes a binary state, where $A_t^p = 0$ indicates an unalarmed state for ant-p at time-step t, and $A_t^p = 1$ signifies an alarmed state. The alarmed state can be communicated from one alarmed ant to others, with conditions defining when an unalarmed ant transitions to an alarmed state.

In a biological context, we describe an ant in an "alarmed" state as having the function of recognizing and alerting the colony to potential threats. This state is behaviorally distinguished by notably elevated walking speeds, increased circular motion, and higher rates of contact compared to the typical behavior in a normally functioning colony [1]. During an actual colony alarm response, only a specific subset of individuals that receive the alarm signal enter this precisely defined behavioral state, while most generally respond by increasing their speed. It is important to note that our characterization of an "alarmed" ant deviates from the strict ethological definition. Instead, it signifies that an ant has received information and responded with some degree of increased speed. In our model, unalarmed ants consistently maintain a mean speed of λ^*. Conversely, alarmed ants exhibit mean speeds greater than λ^*.

3) **Speed Jump Parameter (Λ^p):** If the ant becomes alarmed at any time t, a random number Λ^p is added to her speed parameter λ_t^p. For ant-p, this *speed jump* is defined as the parameter Λ^p. It is randomly sampled once (prior to the simulation) from a truncated exponential distribution because based on anecdotal evidence, the majority of ants are less responsive to alarm information, while a minority display heightened response, thus exponential distribution aligns well with this observation. The distribution has a mean of a^{-1}, and Λ^p takes values within the range of $[0, \Lambda_{max}]$:

$$P(\Lambda^p) = \frac{a\ \exp(-a\Lambda^p)}{1 - \exp(-a\Lambda_{max})}. \tag{2.2}$$

We truncated the tail at Λ_{max} to prevent excessively large, biologically unrealistic speed jumps. The denominator serves to normalize the probability density function. An exponential distribution was chosen because we want to give agents a spread in their intrinsic excitability. We found anecdotally that ants respond differently to alarm information, with some ants being more reactive than others. While we could have used a uniform or normal distribution for speed jump, we noticed that most ants are less responsive, but a few are very responsive. So an exponential distribution matches this observation well.

4) **Speed at Time-step $t+1$ (s_{t+1}^p):** At time-step $t+1$, we determined the value of s_{t+1}^p through random sampling from the exponential distribution with a mean of λ_{t+1}^p (see Figure S4 in the Supplementary file):

$$P(s_{t+1}^p) = \frac{\exp\left(-\frac{s_{t+1}^p}{\lambda_{t+1}^p}\right)}{\lambda_{t+1}^p}. \tag{2.3}$$

5) **Speed Dynamics (λ_{t+1}^p):** The value of λ_{t+1}^p is determined by one of three mutually exclusive conditions, depending on the alarm state of the ant at time-step t. An exception occurs when selecting any of these conditions would lead the ant to exit the physical arena $\left(\text{i.e., } \left(x_{t+1}^p\right)^2 + \left(y_{t+1}^p\right)^2 > 520^2\right)$, in such cases, resampling from an alternative distribution is done, as detailed later.

a) At all time-steps t when ant-p is unalarmed ($A_t^p = 0$), thus, $\lambda_t^p = \lambda^*$.

b) If ant-p did not exhibit alarm at time-step $t-1$ but becomes alarmed at time-step t (i.e., $A_{t-1}^p = 0$ and $A_t^p = 1$), we incorporated her *speed jump* parameter, denoted as Λ^p and constrained within the range $[0, \Lambda_{max}]$, into the baseline speed of the colony. This addition is made to determine the expected speed parameter for this particular ant. It is important to note that this adjustment occurs at most once per simulation, specifically during the initial time-step when the ant enters the alarmed state.

$$\lambda_t^p = \lambda^* + \Lambda^p \tag{2.4}$$

As Λ^p varies among individual ants, a range of responses to alarm signals was expected, reflecting the diversity observed in our empirical trials.

c) If ant-p is alarmed at both time-steps $t-1$ and t (i.e., $A_{t-1}^p = A_t^p = 1$), the following equation governs its expected speed during time-step t:

$$\lambda_t^p = \lambda_{t-1}^p - \beta(\lambda_{t-1}^p - \lambda^*) = \beta\lambda^* + (1-\beta)\lambda_{t-1}^p, \tag{2.5}$$

here, the parameter β, known as the speed decay or speed-loss factor, is an independent parameter for each ant. The specific value of β is determined through fitting the model to experimental data, as explained in Subsection 3.1. This updating rule is derived from our empirical observation that ants with initially higher walking speeds experience a more pronounced reduction in speed during an alarm. Given the higher energetic cost associated with faster speeds, this functional form enables our synthetic ants to prioritize energy conservation, ensuring that faster ants decrease their speed at a comparatively higher rate.

Let $D = \{n \in \mathbb{N} : 1 \leq n \leq N\}$ be the collection of the N ant indexes comprising the whole colony. For each $p \in D$, we defined the neighbors of ant-p at time-step t as the collection of ants (using their indexes as proxy) who are located within r units from ant-p:

$$B_t^p = \left\{k \in D : (x_t^p - x_t^k)^2 + (y_t^p - y_t^k)^2 \leq r^2\right\}. \tag{2.6}$$

Here r represents the alarm signal perceptual radius of any ant. That is, r is the maximum distance at which an ant can sense alarm signals, due to all possible sensory modalities: tactile, vision, and/or olfaction.

We will now briefly summarize now the core model assumptions:

1) Worker-p gets alarmed in time-step $t+1$ whenever one of its B_t^p neighbors is alarmed;

2) There is an abrupt increase in her λ_{t+1}^p (and likewise her sampled speed s_{t+1}^p) when she gets alarmed;

3) The expected value of ant-p's moving speed gradually decays towards the colony's baseline speed after she enters the alarmed state.

2.2. Model initialization

1) We randomly distribute N ants within a two-dimensional circular region with a radius of $M = 520$ pixels. The initial location of ant-p is set as

$$x_0^p = R^p \cos(\theta_1^p), \tag{2.7}$$

$$y_0^p = R^p \sin(\theta_1^p). \tag{2.8}$$

We set R^p uniformly at random from the interval $[0, M]$, and chose θ_1^p uniformly at random from the interval $[0, 2\pi]$.

2) Let $\rho \in (0, 1)$ denote the initial fraction of alarmed ants. We randomly selected a subset $V \subset D$, comprising $[\rho N + 0.5]$ ants (where square brackets indicate the integer value function) to serve as alarm seeds. In other words, $A_1^p = 1$ for all ants in this subset. We established the expected value for their speed as follows:

$$\lambda_1^p = \lambda^{\text{al}} = \lambda^* + \Lambda_{max}. \tag{2.9}$$

Subsequently, the speed s_1^p of each alarm seed ant is stochastically sampled from the exponential distribution with mean λ^{al}, where $P(s) = \frac{1}{\lambda^{\text{al}}} \exp\left(-\frac{s}{\lambda^{\text{al}}}\right)$.

3) Each ant-p in the set $U = D - V$ exists in an unalarmed state represented by $A_1^p = 0$. We establish the expected speed for these ants as $\lambda_1^p = \lambda^*$, and their initial speed s_1^p was randomly selected from an exponential distribution with a mean $\lambda_1^p = \lambda^*$, expressed as $P(s) = \frac{1}{\lambda^*} \exp\left(-\frac{s}{\lambda^*}\right)$.

4) During the first time-step, we relocated the ants from their initial positions to their final positions using the following update formulas:

$$x_1^p = x_0^p + s_1^p \cos(\theta_1^p), \tag{2.10}$$

$$y_1^p = y_0^p + s_1^p \sin(\theta_1^p). \tag{2.11}$$

5) The speed jump parameter for ant-p, denoted as $\Lambda_1^p = \Lambda^p$, was sampled in accordance with Eq (2.2).

This defines the initial parameter set, ϕ_1^p, for ant-p, where $1 \le p \le N$.

2.3. Update procedure

At each time-step t following the initial one (which was initialized above), we iterated through all N ants in the order of their indices. For each ant-p, we modified all components of ϕ_{t-1}^p to ϕ_t^p as outlined below. Subsequently, we proceeded to the next time-step, repeating the process until the final time-step update was completed.

1) The speed jump parameter remained constant for each ant across all time steps, implying that $\Lambda_{t+1}^p = \Lambda_t^p = \Lambda^p$.

2) The heading angle θ_t^p was updated according to the formula $\theta_t^p = \theta_{t-1}^p + \Delta\theta_t^p$, where the value of $\Delta\theta_t^p$ was randomly chosen from the probability function $P(\Delta\theta_{t+1}^p) = \omega\exp(-\omega|\Delta\theta_{t+1}^p|)/2$, as illustrated in Eq (2.1).

3) The update process for the alarm state (A_t^p), expected speed (λ_t^p), and speed of ant-p (s_t^p) to their respective values at time $t + 1$ $(A_{t+1}^p, \lambda_{t+1}^p$, and $s_{t+1}^p)$ is outlined below:

- If A_t^p equals 1, ant-p is already alarmed, and it remains in that alarmed state with A_{t+1}^p being 1. The ant's anticipated speed undergoes an update from λ_t^p through discrete exponential decay, as described in Eq (2.5):

$$\lambda_{t+1}^p = \lambda_t^p - \beta(\lambda_t^p - \lambda^*).$$

  On the other hand, if A_t^p is 0, the alarm state A_{t+1}^p at time $t+1$ is determined by the alarm states of its neighbors B_t^p based on the following two mutually exclusive cases:

  a) If all neighbors B_t^p of ant-p are unalarmed, we set $A_{t+1}^p = 0$ and maintain the ant's expected speed unchanged:

$$\lambda_{t+1}^p = \lambda^*.$$

  b) If at least one of ant-p's neighbors B_t^p is alarmed, we set $A_{t+1}^p = 1$. In this case, we also increase the ant's expected speed by her speed jump:

$$\lambda_{t+1}^p = \lambda^* + \Lambda^p.$$

- The speed, s_{t+1}^p, is determined by randomly sampling from the exponential distribution with a mean of λ_{t+1}^p, as specified in Eq (2.3).

4) The position (x_t^p, y_t^p) undergoes an update to (x_{t+1}^p, y_{t+1}^p) in one of two ways, depending on whether the proposed new position:

$$\tilde{x}_{t+1}^p = x_t^p + s_{t+1}^p \cos(\theta_{t+1}^p),$$
$$\tilde{y}_{t+1}^p = y_t^p + s_{t+1}^p \sin(\theta_{t+1}^p),$$

lies outside the arena. If the new position is inside or on the boundary of the arena, such that $|(\tilde{x}_{t+1}^p, \tilde{y}_{t+1}^p)| \leq M$, then:

$$x_{t+1}^p = \tilde{x}_{t+1}^p,\ y_{t+1}^p = \tilde{y}_{t+1}^p.$$

If the new position falls outside the region defined by $|(\tilde{x}_{t+1}^p, \tilde{y}_{t+1}^p)| > M$, the ant is redirected inward as follows:

$$x_{t+1}^p = x_t^p - s_{t+1}^p \cos(\theta_{t+1}^p),\ y_{t+1}^p = y_t^p - s_{t+1}^p \sin(\theta_{t+1}^p).$$

Subsequently, θ_{t+1}^p is updated to account for the new orientation of the velocity vector:

$$\theta_{t+1}^p = \cos^{-1}\left[\frac{x_{t+1}^p - x_t^p}{s_{t+1}^p}\right].$$

The detailed procedure for each update following initialization can be elucidated using the schematic depicted in Figure 1.

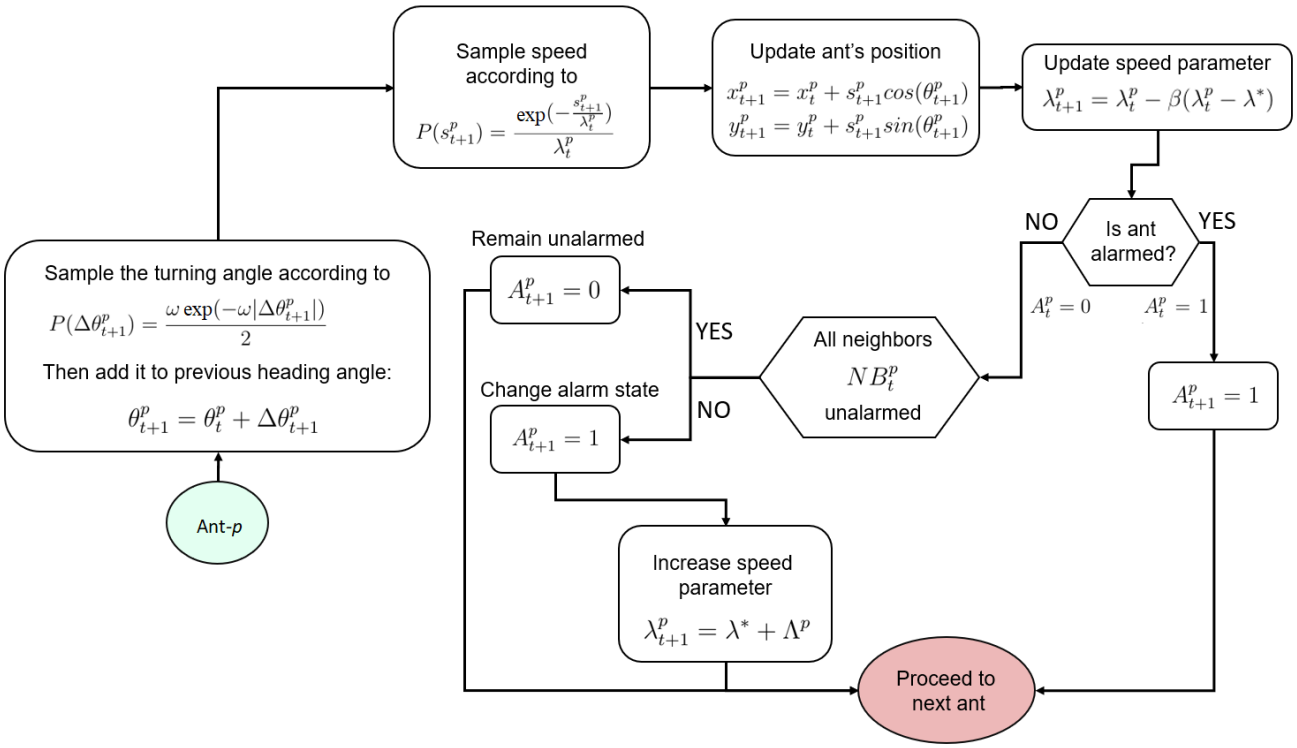

Figure 1. A schematic illustrating the process of updating the characteristic parameters of an individual ant at a specific time-step. The turning angle $\Delta\theta^p_{t+1}$ is selected from a Laplace distribution with a location parameter of 0 and a scale parameter of $\frac{1}{\omega}$ as described in Eq (2.1). Additionally, the speed s^p_{t+1} is chosen from an exponential distribution with an average of λ^p_t according to Eq (2.3), and the speed jump Λ^p is selected from a truncated exponential distribution with an average of a^{-1} as outlined in Eq (2.2).

3. Model validation and results

In this section, we first employed the empirical data available in [1] to validate our model. Then, we conducted systematic simulations to investigate the influence of crucial parameters on the dynamics of group mean speed.

3.1. Model validation

There are three set of data for three different colonies A, B, and C in [1]. For each colony, we adjusted our model to match the empirical data both before and after the introducing seed alarmed ants, as explained in [1], to find parameters λ^*, r, a, and β as shown in Figure 2. All remaining parameters were held constant, following the specifications in Table 1. To perform the fitting process, we utilized MATLAB's fminsearch function, employing the simplex search method developed by Lagarias et al. [27]. This approach aimed to minimize the error between the model's simulation and the actual data, as detailed in Table 1.

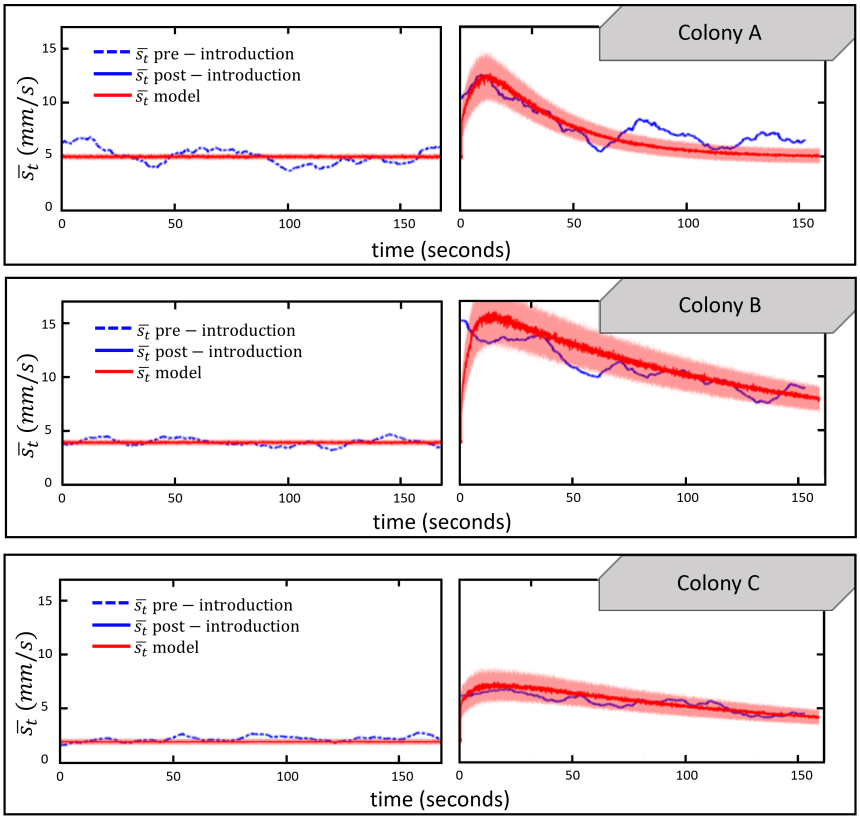

Figure 2. The average speed of the group, denoted as $\overline{s_t}$, is depicted through blue lines in both pre- and post-introduction videos: The red circles represent the average curve derived from 300 replicates of the model under fitted parameters, with error bands indicating standard deviation across replicates. The model parameters utilized are detailed in Tables 1 and 2. All curves have been smoothed for clarity. Notably, the post-introduction data is plotted immediately after the pre-introduction data to facilitate comparison, with the 25-minute gap omitted for simplicity.

Table 1. Initialization, movement, and contact parameters: The baseline values provided were applied consistently across all replicates and figures, unless specified otherwise.

Symbol	Description	Baseline value	Estimated using
T	Total time-steps in simulation	4500 (150 s)	Video duration
M	Radius of arena	520 pxl (75.5 mm)	Empirical arena
N	Population size	60	Empirical population
ω^{-1}	Mean turning angle	21.14°	Empirical data
r	Radius within which an interaction occurs	58.27 pxl (5.8 mm)	Model fitting
λ^*	Steady state speed parameter	1.8739 pxl/time-step (8.16 mm/s)	Pre-introduction $\overline{s_t^p}$
Λ_{max}	Maximum increase in λ due to excitation	6.88 pxl/time-step (30 mm/s)	Empirical data
a	Decay rate of $P(\Lambda^p)$ over Λ^p	0.1497	Model fitting
β	Decay rate of λ^p over time	0.00032	Model fitting
ρ	Fraction of colony initially alarmed	0.05	Empirical data

Table 2. Predictions for the parameters of our colonies' model: The parameter vector (λ^*, r, a, β) for each colony was adjusted to minimize the combined root mean square error $(RMSE_{pre-introduction} + RMSE_{post-introduction})$ between experimental and model-predicted values of $\overline{s_t}$, while keeping all other parameters fixed based on Table 1. The averages of each column served as the default parameters in Table 1.

Colony	λ^* $(pxls/frame)$	r $(pxls)$	a	β
A	1.149 ± 0.046	40 ± 3	0.100 ± 0.007	$1.00 \times 10^{-3} \pm 1 \times 10^{-5}$
B	0.918 ± 0.045	60 ± 3	0.060 ± 0.006	$2.5 \times 10^{-4} \pm 1 \times 10^{-5}$
C	0.0459 ± 0.044	61 ± 3	0.250 ± 0.005	$2.2 \times 10^{-4} \pm 1 \times 10^{-5}$

We defined the framewise group mean speed as $\overline{s_t} = \frac{1}{N}\sum_{p=1}^{N} s_t^p$, where N represents the group size, and time-averaged speeds as $\overline{s^p} = \frac{1}{T}\sum_{t=1}^{T} s_t^p$, where T is the total number of time-steps.

The blue curves in Figure 2 depict framewise group mean speeds $(\overline{s_t})$ both before and after the introduction. Meanwhile, the red curves represent the model's $\overline{s_t}$, averaged across 300 model replicates. These replicates, described in Section 2.2, are initialized with randomized starting positions (x_0^p, y_0^p), speeds s_0^p, and orientations θ_0^p. It is important to note that for pre-introduction replicates, the fraction of the colony initially alarmed (ρ) was set to zero. The fitted parameters used in the model are summarized in Table 2 and offer a rough estimate of each colony's true latent parameters.

In Figure 2, the group mean speed, denoted as $\overline{s_t}$, exhibits a tendency to rise rapidly and decline gradually, with variations in the alarm response among different colonies. A comparison between the empirical results and our fitted model reveals that the model exhibits the necessary flexibility to capture this range of colony responses. In a biological context, the typical pattern of swift speed increase and slower speed decrease can be interpreted as ants quickly getting agitated upon initial exposure to alarm signals. This rapid response to the stimulus presumably enables the colony to react promptly to potential threats. The decay phase in the colony's response indicates that although ants take a longer time to return to a calm state, they do revert to their baseline behavior within a few minutes unless subjected to another alarm stimulus. Due to the positive linear relationship between energetic cost of locomotion and speed [28, 29], the ability to swiftly return to baseline states allows colonies to minimize energy expenditure on false alarms and reduce the disruption of normal colony function caused by an alarm event.

Figure 3(a) illustrates histograms that aggregate post-introduction speed data from colonies A, B, and C, divided into five non-overlapping, 30-second windows. On the horizontal axis, individual framewise speeds s_t^p are binned, while the vertical axis depicts the frequency of s_t^p within each bin, aggregated over each 30-second time window. The frequencies were normalized to represent a probability density function and plotted on a linear scale (with insets in semilog scale).

In Figure 3(b), all parameters were fixed according to Table 1. We conducted 300 model replicates and pooled s_t^p from all replicates. The parameters in Table 1 were carefully chosen to closely calibrate the model to the spatial and time scales observed in the pooled post-introduction videos. Each curve in Figure 3(b) represents data aggregated from a 30-second window (equivalent to 900 simulation time-steps) and displays the probability distribution over s_t^p. The empirical distributions in Figure 3(a) encompass a total of 670,680 data points, while the model distributions in Figure 3(b) comprise approximately 81 million points.

Comparing the dynamics of speed distribution between Figure 3(a),(b) reveals that the distributions maintained an exponential pattern throughout both post-introduction videos and model replicates. Beyond the initial 30-second interval, the slope of the distribution progressively becomes more negative. This suggests that ants are converging toward a specific baseline distribution characterized by a lower mean and variance. In the context of the selected parameters (see Table 1), the decay of the distribution occurs roughly on comparable time scales.

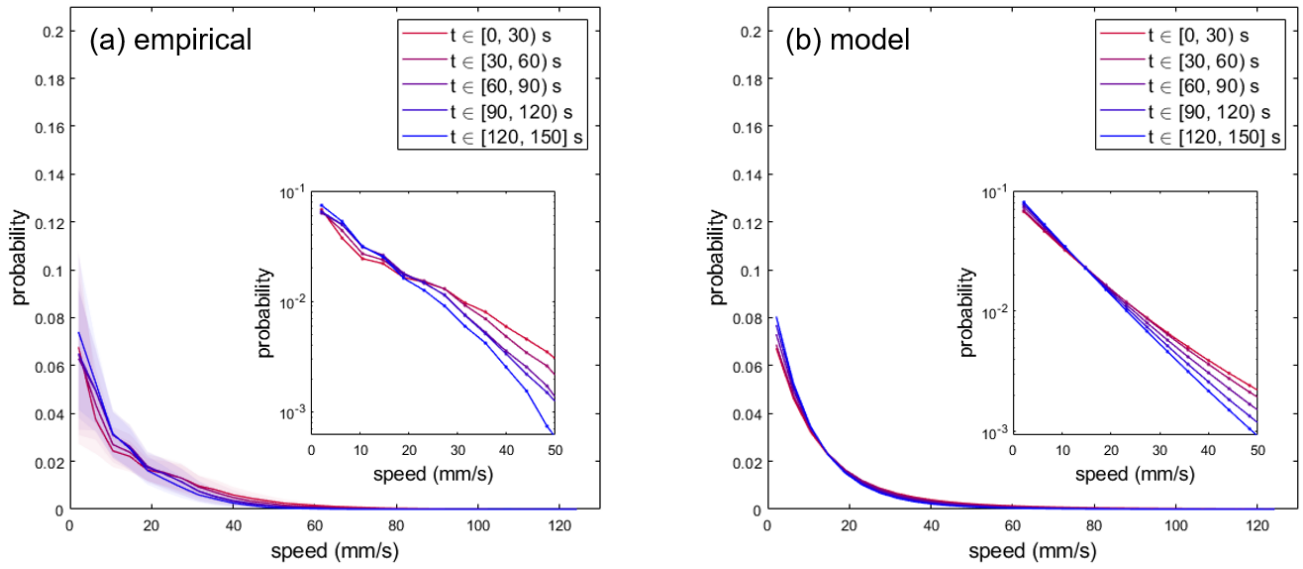

Figure 3. Depicted speed distributions within consecutive 30-second time intervals for (a) combined empirical trials post-introduction and (b) 300 aggregated model replicates: Each curve illustrates the histogram of individual framewise speeds (s_t^p) within the respective 30-second time window. Error bands, where visible, represent the standard error. Insets display the same distributions on semilogarithmic axes, truncated to highlight the speed range of 0 to 50 mm/s. In both experimental and model scenarios, the distribution approximates an exponential pattern with a diminishing tail over time. Refer to Table 1 for the parameters employed in the aforementioned replicates.

3.2. Dynamical outcomes

Here, we initially investigate the influence of colony size (N), or equivalently, the spatial density of individuals, on the dynamics of alarm spread. We gain insights into how increasing group sizes might impact the colony-level alarm response by observing its effect on several speed-based metrics. Next, we individually vary each of the other model parameters and observe how they affect the dynamics of $\overline{s_t}$ (Figure 4). Each plot in this section is derived from averaging 300 model replicates.*

*The parameter settings for all figures align with those in Table 1. The initial conditions are uniform across all simulations, except for randomizing starting positions (x_0^p, y_0^p), speeds s_0^p, and orientations θ_0^p.

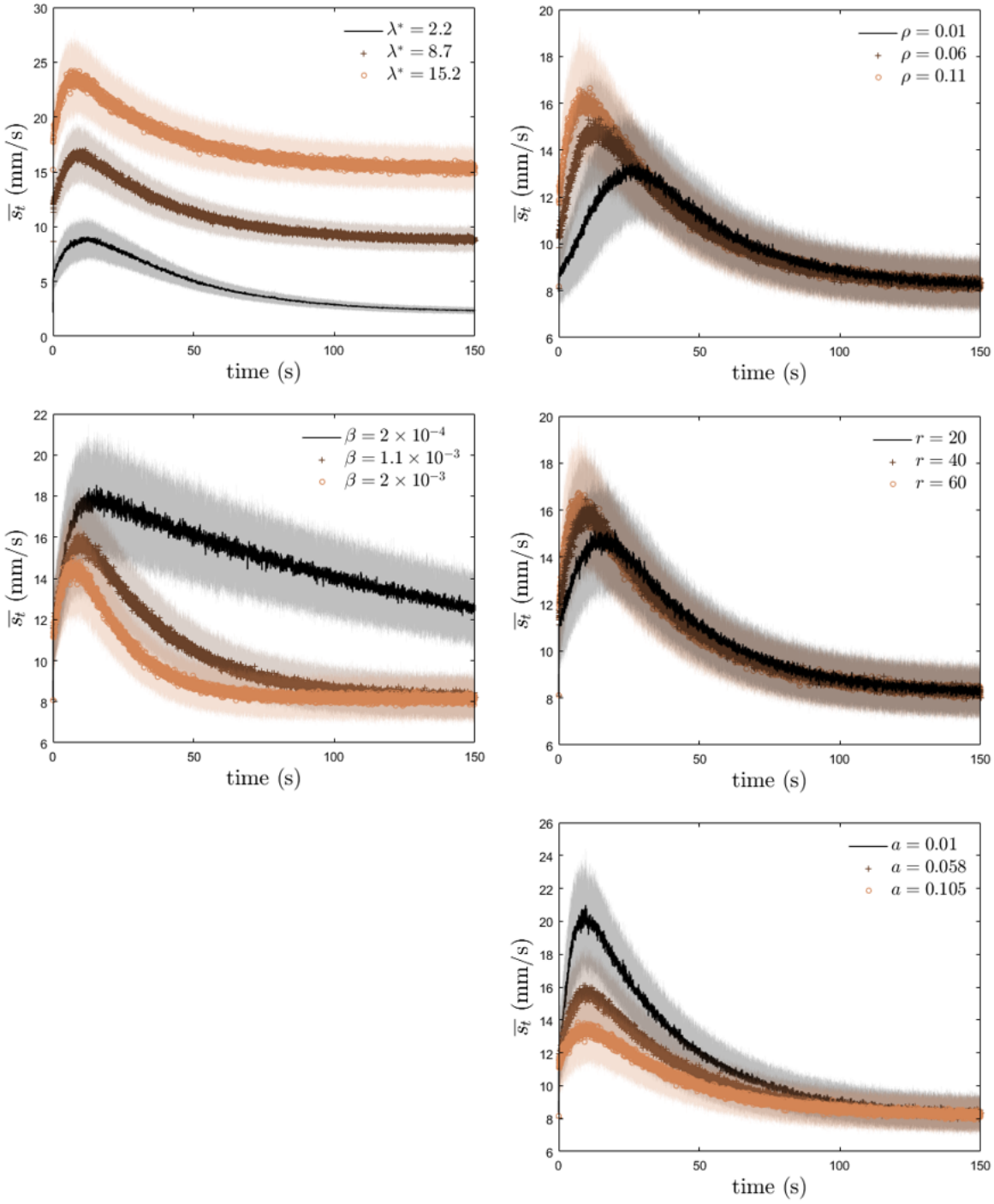

Figure 4. The mean curve $\overline{s_t}$ averaged over 300 replicates: The error bands depict the standard deviation across replicates. For details regarding the parameters employed in all replicates, excluding the one undergoing variation, refer to Table 1.

In Figure 5, we scrutinized three metrics of the degree of alarm excitation: colony mean speed ($\overline{s_t}$), colony expected mean speed parameter ($\overline{\lambda_t}$), and the fraction of alarmed ants. The curves depict the dynamics at three colony sizes ($N = 20, 60, 180$), with the horizontal axis representing time converted

from simulation time-steps to seconds. For this set of results only, we introduced the alarm seed ants at time-step $t_0 = 720 = 24\ s$ to clarify the speed growth phase. The "fraction of colony alarmed" in Figure 5(c) represents the number of individuals in the state $A_t^p = 1$, divided by N. According to all three metrics, the model predicts that increased density would lead to a more rapid spread and decay of alarm.

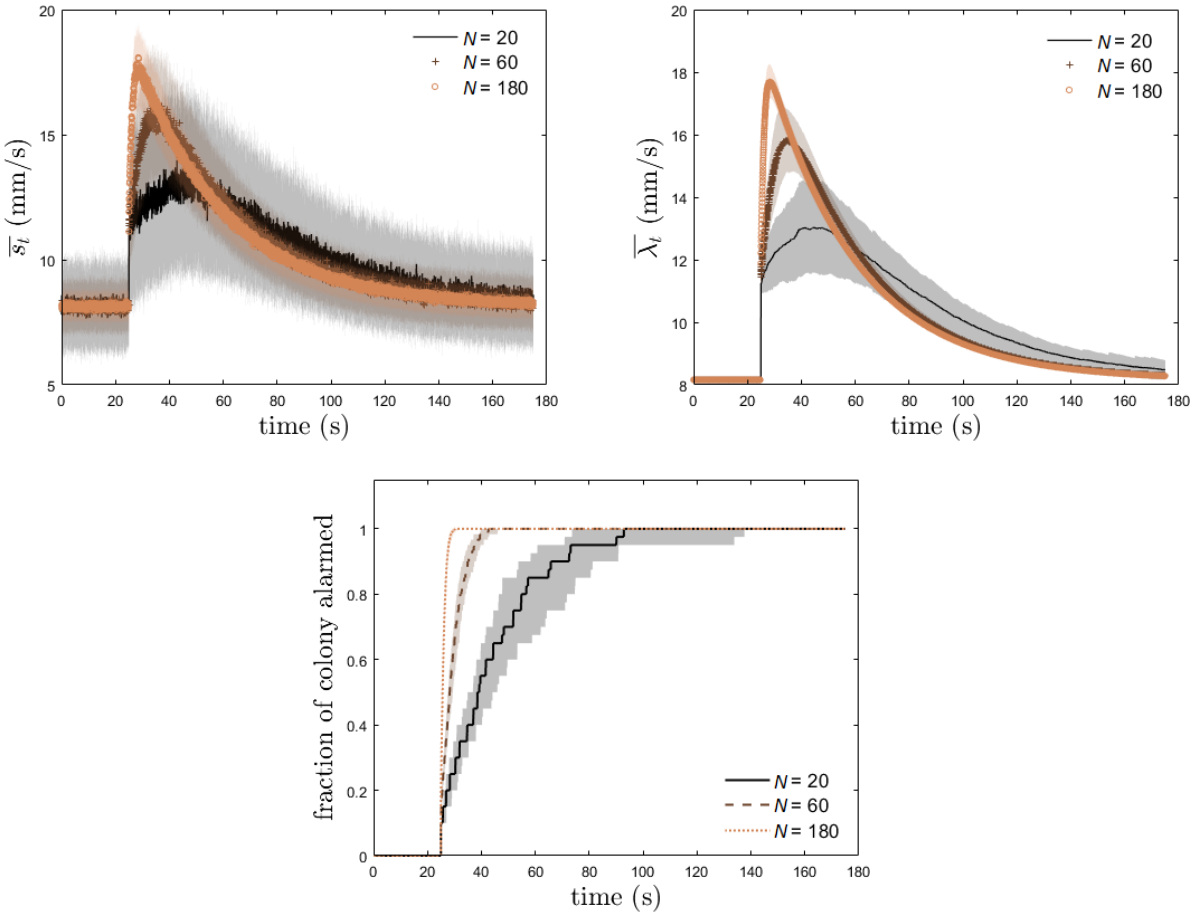

Figure 5. The impact of group size on the dynamics of the group mean speed (top left), the group expected mean speed parameter (top right), and the fraction of the group alarmed (bottom): A larger group size implies higher density, given that the size of the arena is fixed. Increased density results in a more rapid overall propagation of alarm. The curves in the top and middle panels represent the means of 300 replicates, with their corresponding standard deviations depicted in shaded regions. In the bottom panel, the curves illustrate the first quartile (Q1), second quartile (Q2), and third quartile (Q3) of 300 replicates, along with their standard deviations. Default parameters from Table 1 were used for all plots.

The result also suggests that the group mean speed ($\overline{s_t}$) should reach a higher peak in denser groups. Table 3 lists each group's "peak height", defined as $max\overline{s_t} - \lambda^*$. Each value in the peak height column is then normalized by the $N = 20$ group's peak height for ease of comparison. Increasing N by factors of 3 and 9 led to 1.55 times and 1.92 times increases in peak height, respectively. These peaks also occurred at earlier times. "Time-to-peak" was computed as $t_{peak} - t_0$, where t_{peak} is the time of maximum

$\overline{s_t}$ and $t_0 = 720$ time-steps is the time at which the alarmed ants were introduced. All values in the time-to-peak column were normalized by the time-to-peak of the $N = 20$ group. The last column lists the fraction of ants alarmed at t_{peak}.

Table 3. Metrics for colony alarm levels across three colony sizes: "Peak height" denotes the maximum group mean speed, represented as $\overline{s_t}$. "Time-to-peak" measures the duration between introducing alarmed ants (at t_0) and reaching the maximum speed. "Fraction alarmed at peak" indicates the proportion of alarmed ants at the peak time divided by N. All peak heights and time-to-peaks were normalized based on the values for the $N = 20$ group for ease of comparison.

N	Scale factor	Peak height	Time to peak	Fraction alarmed at peak
20	1	1.000 ± 0.147	1	0.590 ± 0.015
60	3	1.549 ± 0.162	0.403	0.845 ± 0.010
180	9	1.920 ± 0.170	0.108	0.915 ± 0.010

Table 3 illustrates that, according to our assumptions, a more densely populated environment expedites the rapid dissemination of the initial alarm signal within the group. The $N = 180$ group reached its peak excitation in only one-tenth of the time required by the $N = 20$ group. Moreover, at the peak time, the $N = 180$ group exhibited an alarm response in 91.5% ± 1% of ants, while the $N = 20$ group had only 59% ± 1.5% alarmed. It is crucial to acknowledge that the model may overestimate the actual increases in the rate of spread and the maximum excitation at higher densities. This overestimation is attributed to the model not accounting for pauses in motion that may occur during ant-to-ant interactions.

In Figure 4, we systematically varied each fitted parameter individually while keeping the others constant, as outlined in Table 1. Our observations revealed that augmenting either the contact radius, denoted as r (see panel 4), or the initially alarmed fraction, denoted as ρ (see panel 2), had analogous effects on the dynamics of $\overline{s_t}$ compared to increasing the parameter N. This manifested in a quicker rise, a faster decay, and a higher peak of $\overline{s_t}$. These outcomes align with intuitive expectations. A larger contact radius (r) facilitates a swifter alarm spread due to more frequent contacts, while introducing a greater fraction (ρ) of initially alarmed ants enhances the stimulus and accelerates signal transmission within the group.

In Figure 4, panel 5, we observe that reducing the parameter a (resulting in an increased variation in speed jumps, Λ^p, among individual ants) leads to higher peak heights without significant differences in time-to-peak. Similarly, substantial increases in group baseline speed, λ^* (panel 1), do not result in earlier peaks in excitation. An elevated decay rate of the expected speed, regulated by the parameter β, leads to a decrease in the group's mean speed $\bar{s}_t$. It attains a lower peak and subsequently declines to the baseline of 8.16 mm/s at a faster rate. This outcome aligns with the model assumption that as β increases, the time-series of expected speed diminishes (refer to Eq (2.5)). Consequently, this phenomenon signals a reduction in alarmed ant speeds, subsequently impacting the overall group mean speed. Regardless of the chosen parameter values we explored, the model consistently exhibits a swift rise and gradual decay of $\overline{s_p}$, aligning with observations from post-introduction videos. This consistency in model behavior reinforces the validity of our underlying assumptions regarding alarm signal transmission and damping.

4. Discussion and conclusions

In formulating the model, we incorporated several crucial empirical observations regarding ant colony alarm responses: (i) the swift onset of alarm excitation, (ii) the diversity in individual-level responses during an alarm, and (iii) the relatively gradual decay of alarm. Since speed is the movement feature most strongly correlated with alarm [1], we investigated the role of this behavior in regulating alarm. Our model employed a parallel set of three individual-level speed adjustment mechanisms, collectively designed to replicate the observed group-level speed distribution dynamics (Figure 3(a)).

The first mechanism bestowed upon the ants is a switch-like response to alarm signals: They rapidly increase speed upon encountering alarmed nestmates, and this increase varies among individuals. An alternative mechanism could involve ants gradually increasing their speed in proportion to the strength or frequency of received alarm signals. Several studies examining the role of encounter rate [30–32] and signal strength [33] on task recruitment in ant species suggest that ants have the potential for a more modulated response. The use of quorum rules by some house-hunting ants [34, 35] implies that alarm-susceptible ants might be aggregating data from multiple contacts as well.[†] While such mechanisms are conceivable, our results underscore that an instantaneous speed jump upon close contact is sufficient to capture the extremely rapid rise in $\overline{s_t}$ in the initial phase of the alarm response, as shown in Figure 2. This rapid initial response also proved highly robust when varying each data-fitted model parameter individually, as demonstrated in Figure 4.

The second key assumption revolved around the variability in the response (speed increase) of our ants when alarmed. Notably, individual variations among ants within the same colony, and even within the same task group, have been well-documented in various contexts such as task performance [36], task specialization [37], and activity level [38]. This behavioral diversity has been attributed to phenotypic, age-based [39], physiological (Flexible Task Allocation), and experiential differences [40].

Our observations indicate that ants exhibit diverse responses during alarm situations (Section 3.2). We postulated that allowing individuals to increase their speed by different amounts, denoted as Λ^p, during alarms may lead to similar effects on the group-level, framewise speed distributions as observed in post-introduction videos (Figure 3). In the initial 30 seconds (red curve, Figure 3(a)), the histogram slope is relatively higher than at baseline (blue curve, Figure 3(a)), indicating a thicker-tailed speed distribution with a higher mean, $\overline{s_t^p}$, and greater variance in s_t^p during the peak of alarm. Our model's assumptions regarding the variation in individuals' Λ^p (Eq (2.2)) contribute to this initial shift in the framewise speed distribution.

Additionally, during the decay phase of the alarm response, we discovered that allowing alarmed ants to decrease their current average speed λ_t^p at a rate proportional to $\lambda_t^p - \lambda^*$ was sufficient to capture the decay of the framewise speed distribution toward its baseline (Figure 3). The gradual decrease in the distribution's mean $\overline{s_t}$ under most parameter settings supports our assumptions about ants' consistent prioritization of energy conservation. Since moving at high speeds consumes more energy, faster-moving ants tend to decrease their speed more rapidly. It is worth noting that both empirical data in [1] and model data indicate that the individual's speed over consecutive time-steps is not monotonic. However, on average, the speed increases when ants are alarmed and decreases

[†]We tested a model version based on these rules (unpublished data) and obtained reasonable but less-accurate agreement with the empirical videos.

afterward. This suggests that decay of the individual excitement state mediates alarm decay at the group level most effectively.

We contribute several unique features in the context of other self-propelled particle models. Most notable is the mechanism that allows agents to adapt to new information. When an agent receives the alarm signal, it modulates its behavior by changing its speed parameter λ_t^p. This affects the distribution from which the agent samples its speed. This distribution then continues to shift over time, as the speed parameter decays post-alarm. Allowing adaptive speed distributions is not common in self-propelled particles, but was essential to capture the dynamics in our alarm experiment.

Discrepancies between empirical dynamics and model output partly stem from the model's lack of realism in depicting ant movement. For instance, in actuality, ants commonly pause during encounters with nestmates, a behavior omitted in the model for the sake of simplicity. Additionally, the model employs a random sampling approach for ant speeds at each time-step, neglecting the likely correlation between speeds in consecutive frames. This absence of speed correlation in the model results in a much smoother decay in $\overline{s_t}$ compared to pre- and post-introduction trials (Figure 2, Supplemental Videos). These movement characteristics constrain the accuracy of group-level dynamics, and future research should aim to model individual-level movement more precisely. Approaches such as machine-learning-based regression models, recurrent neural networks, or reinforcement learning methods could be employed to train models that accurately represent the velocity vector of each agent sequentially.

The ant colony's alarm response presents an excellent avenue for investigating adaptive information flow and signaling mechanisms in animal groups and other complex systems. This system is amenable to experimental manipulation, and agent-based modeling allows for the prototyping of individual signal-response rules. Although closely linked to the existing body of work on collective motion [21, 23, 26, 41, 42] and general infection processes, this study stands out as one of the few examinations of insect alarm behavior utilizing object tracking. Through simulating variations in a natural colony, we aimed to offer biological insights into the latent factors influencing a colony's alarm response. Moreover, the proposed mechanisms of signal transmission and decay in the model are likely applicable to other systems where transmission is instantaneous, and the group response is adaptive.

Use of AI tools declaration

The authors declare they have not used Artificial Intelligence (AI) tools in the creation of this article.

Acknowledgments

This work was supported by the NSF-DMS (Award Number 1716802); the NSF-IOS/DMS (Award Number 1558127); the James S. McDonnell Foundation 21st Century Science Initiative in Studying Complex Systems Scholar Award (UHC Scholar Award 220020472); and the Defense Advanced Research Projects Agency (DARPA)-SBIR (2016.2 SB162-005). We would like to thank the members of the Fewell lab for their assistance in ant rearing and for their feedback on the manuscript.

Conflict of interest

The authors declare there is no conflict of interest.

References

1. X. Guo, M. R. Lin, A. Azizi, L. P. Saldyt, Y. Kang, T. P. Pavlic, et al., Decoding alarm signal propagation of seed-harvester ants using automated movement tracking and supervised machine learning, *Proc. R. Soc. B*, **289** (2022), 20212176. https://doi.org/10.1098/rspb.2021.2176
2. O. Feinerman, A. Korman, Individual versus collective cognition in social insects, *J. Exp. Biol.*, **220** (2017), 73–82. https://doi.org/10.1242/jeb.143891
3. B. Doerr, M. Fouz, T. Friedrich, Why rumors spread fast in social networks, *Commun. ACM*, **55** (2012), 70–75. https://doi.org/10.1145/2184319.2184338
4. L. Bonnasse-Gahot, H. Berestycki, M. Depuiset, M. B. Gordon, S. Roché, N. Rodriguez, et al., Epidemiological modelling of the 2005 french riots: A spreading wave and the role of contagion, *Sci. Rep.*, **8** (2018), 107. https://doi.org/10.1038/s41598-017-18093-4
5. D. A. Sprague, T. House, Evidence for complex contagion models of social contagion from observational data, *PLoS One*, **12** (2017), 1–12. https://doi.org/10.1371/journal.pone.0180802
6. C. E. Coltart, B. Lindsey, I. Ghinai, A. M. Johnson, D. L. Heymann, The ebola outbreak, 2013–2016: Old lessons for new epidemics, *Phil. Trans. R. Soc. B*, **372** (2017), 20160297. https://doi.org/10.1098/rstb.2016.0297
7. B. Hölldobler, E. O. Wilson, *The Ants*, Harvard University Press, 1990.
8. F. E. Regnier, E. O. Wilson, The alarm-defence system of the ant acanthomyops claviger, *J. Insect Physiol.*, **14** (1968), 955–970. https://doi.org/10.1016/0022-1910(68)90006-1
9. W. H. Bossert, E. O. Wilson, The analysis of olfactory communication among animals, *J. Theor. Biol.*, **5** (1963), 443–469. https://doi.org/10.1016/0022-5193(63)90089-4
10. E. Frehland, B. Kleutsch, H. Markl, Modelling a two-dimensional random alarm process, *BioSystems*, **18** (1985), 197–208. https://doi.org/10.1016/0303-2647(85)90071-1
11. D. J. McGurk, J. Frost, E. J. Eisenbraun, K. Vick, W. A. Drew, J. Young, Volatile compounds in ants: Identification of 4-methyl-3-heptanone from *Pogonomyrmex* ants, *J. Insect Physiol.*, **12** (1966), 1435–1441. https://doi.org/10.1016/0022-1910(66)90157-0
12. J. B. Xavier, J. M. Monk, S. Poudel, C. J. Norsigian, A. V. Sastry, C. Liao, et al., Mathematical models to study the biology of pathogens and the infectious diseases they cause, *Iscience*, **25** (2022), 104079. https://doi.org/10.1016/j.isci.2022.104079
13. P. Törnberg, Echo chambers and viral misinformation: Modeling fake news as complex contagion, *PLoS One*, **13** (2018), 1–21. https://doi.org/10.1371/journal.pone.0203958
14. G. I. Marchuk, *Mathematical Modelling of Immune Response in Infectious Diseases*, Springer, 2013. https://doi.org/10.1007/978-94-015-8798-3
15. L. G. de Pillis, A. E. Radunskaya, A mathematical model of immune response to tumor invasion, in *Computational Fluid and Solid Mechanics 2003*, Elsevier, (2003), 1661–1668. https://doi.org/10.1016/B978-008044046-0.50404-8

16. L. G. de Pillis, A. Eladdadi, A. E. Radunskaya, Modeling cancer-immune responses to therapy, *J. Pharmacokinet. Pharmacodyn.*, **41** (2014), 461–478. https://doi.org/10.1007/s10928-014-9386-9

17. A. M. Smith, Validated models of immune response to virus infection, *Curr. Opin. Syst. Biol.*, **12** (2018), 46–52. https://doi.org/10.1016/j.coisb.2018.10.005

18. J. M. Conway, R. M. Ribeiro, Modeling the immune response to hive infection, *Curr. Opin. Syst. Biol.*, **12** (2018), 61–69. https://doi.org/10.1016/j.coisb.2018.10.006

19. S. Legewie, N. Blüthgen, H. Herzel, Mathematical modeling identifies inhibitors of apoptosis as mediators of positive feedback and bistability, *PLoS Comput. Biol.*, **2** (2006), e120. https://doi.org/10.1371/journal.pcbi.0020120

20. T. Fasciano, H. Nguyen, A. Dornhaus, M. C. Shin, Tracking multiple ants in a colony, in *2013 IEEE Workshop on Applications of Computer Vision (WACV)*, IEEE, (2013), 534–540. https://doi.org/10.1109/WACV.2013.6475065

21. C. W. Reynolds, Flocks, herds and schools: A distributed behavioral model, in *SIGGRAPH '87: Proceedings of the 14th Annual Conference on Computer Graphics and Interactive Techniques*, ACM, (1987), 25–34. https://doi.org/10.1145/37401.37406

22. T. Vicsek, A. Czirók, E. Ben-Jacob, I. Cohen, O. Shochet, Novel type of phase transition in a system of self-driven particles, *Phys. Rev. Lett.*, **75** (1995), 1226–1229. https://doi.org/10.1103/PhysRevLett.75.1226

23. H. Chaté, F. Ginelli, G. Grégoire, F. Raynaud, Collective motion of self-propelled particles interacting without cohesion, *Phys. Rev. E*, **77** (2008), 046113. https://doi.org/10.1103/PhysRevE.77.046113

24. I. D. Couzin, J. Krause, R. James, G. D. Ruxton, N. R. Franks, Collective memory and spatial sorting in animal groups, *J. Theor. Biol.*, **218** (2002), 1–11. https://doi.org/10.1006/jtbi.2002.3065

25. H. S. Fisher, L. Giomi, H. E. Hoekstra, L. Mahadevan, The dynamics of sperm cooperation in a competitive environment, *Proc. R. Soc. B*, **281** (2014), 20140296. https://doi.org/10.1098/rspb.2014.0296

26. H. Hildenbrandt, C. Carere, C. K. Hemelrijk, Self-organized aerial displays of thousands of starlings: A model, *Behav. Ecol.*, **21** (2010), 1349–1359. https://doi.org/10.1093/beheco/arq149

27. J. C. Lagarias, J. A. Reeds, M. H. Wright, P. E. Wright, Convergence properties of the nelder–mead simplex method in low dimensions, *SIAM J. Optim.*, **9** (1998), 112–147. https://doi.org/10.1137/S1052623496303470

28. A. Lipp, H. Wolf, F. Lehmann, Walking on inclines: Energetics of locomotion in the ant Camponotus, *J. Exp. Biol.*, **208** (2005), 707–719. https://doi.org/10.1242/jeb.01434

29. N. C. Holt, G. N. Askew, Locomotion on a slope in leaf-cutter ants: Metabolic energy use, behavioural adaptations and the implications for route selection on hilly terrain, *J. Exp. Biol.*, **215** (2012), 2545–2550. https://doi.org/10.1242/jeb.057695

30. M. J. Greene, D. M. Gordon, Interaction rate informs harvester ant task decisions, *Behav. Ecol.*, **18** (2007), 451–455. https://doi.org/10.1093/beheco/arl105

31. D. M. Gordon, N. J. Mehdiabadi, Encounter rate and task allocation in harvester ants, *Behav. Ecol. Sociobiol.*, **45** (1999), 370–377. https://doi.org/10.1007/s002650050573

32. D. M. Gordon, The regulation of foraging activity in red harvester ant colonies, *Am. Nat.*, **159** (2002), 509–518. https://doi.org/10.1086/339461
33. N. Razin, J. Eckmann, O. Feinerman, Desert ants achieve reliable recruitment across noisy interactions, *J. R. Soc. Interface*, **10** (2013), 20130079. https://doi.org/10.1098/rsif.2013.0079
34. S. C. Pratt, Behavioral mechanisms of collective nest-site choice by the ant *Temnothorax curvispinosus*, *Insect. Soc.*, **52** (2005), 383–392. https://doi.org/10.1007/s00040-005-0823-z
35. S. C. Pratt, Quorum sensing by encounter rates in the ant *Temnothorax albipennis*, *Behav. Ecol.*, **16** (2005), 488–496. https://doi.org/10.1093/beheco/ari020
36. A. Dornhaus, Specialization does not predict individual efficiency in an ant, *PLoS Biol.*, **6** (2008), e285. https://doi.org/10.1371/journal.pbio.0060285
37. S. N. Beshers, J. H. Fewell, Models of division of labor in social insects, *Annu. Rev. Entomol.*, **46** (2001), 413–440. https://doi.org/10.1146/annurev.ento.46.1.413
38. D. Charbonneau, C. Poff, H. Nguyen, M. C. Shin, K. Kierstead, A. Dornhaus, Who are the "lazy" ants? The function of inactivity in social insects and a possible role of constraint: Inactive ants are corpulent and may be young and/or selfish, *Integr. Comp. Biol.*, **57** (2017), 649–667. https://doi.org/10.1093/icb/icx029
39. A. Bernadou, J. Busch, J. Heinze, Diversity in identity: Behavioral flexibility, dominance, and age polyethism in a clonal ant, *Behav. Ecol. Sociobiol.*, **69** (2015), 1365–1375. https://doi.org/10.1007/s00265-015-1950-9
40. E. J. H. Robinson, T. O. Richardson, A. B. Sendova-Franks, O. Feinerman, N. R. Franks, Radio tagging reveals the roles of corpulence, experience and social information in ant decision making, *Behav. Ecol. Sociobiol.*, **63** (2009), 627–636. https://doi.org/10.1007/s00265-008-0696-z
41. H. G. Tanner, A. Jadbabaie, G. J. Pappas, Stable flocking of mobile agents, part I: Fixed topology, in *42nd IEEE International Conference on Decision and Control*, IEEE, (2003), 2010–2015. https://doi.org/10.1109/CDC.2003.1272910
42. A. Kolpas, M. Busch, H. Li, I. D. Couzin, L. Petzold, J. Moehlis, How the spatial position of individuals affects their influence on swarms: A numerical comparison of two popular swarm dynamics models, *PloS One*, **8** (2013), e58525. https://doi.org/10.1371/journal.pone.0058525

AIMS Press